Ultra-High-Contrast and Tunable-Bandwidth Filter Using Cascaded High-Order Silicon Microring Filters

Jun Rong Ong, *Student Member, IEEE*, Ranjeet Kumar, *Student Member, IEEE*, and Shayan Mookherjea, *Senior Member, IEEE*

***Abstract*— High-contrast optical filtering is demonstrated using cascaded silicon microrings. We report an experimental measurement of a record 100 dB pass-band to stop-band contrast, tunable 12-125 GHz passband full-width at half-maximum, band-center insertion loss ripple <3 dB, and a group delay ripple <5 ps, using transverse electric polarized light.**

***Index Terms*— Integrated optics, optical filters.**

I. Introduction

In LIGHTWAVE communications systems, many of which are based on some form of spectral multiplexing, a compact filter is widely used in wavelength division multiplexing and add/drop functions [1]–[3], channel routing and switching [4]–[6], optical signal processing [7], [8], energy-efficient optical networks [9], etc. Chip-scale silicon photonic circuits enable significant size, weight and energy savings. However, at the high end of the scale, the performance of silicon photonic filters has lagged behind their off–chip counterparts; measurements report (see Table I) about 30-50 dB contrast compared to greater than 60 dB contrast which is available in off-chip systems such as diffractive grating spectrometers, cascaded fiber Bragg grating filters or tabletop diffraction-based instruments. High contrast is particularly useful in LIDAR, nonlinear wavelength conversion, nonlinear microscopy, astronomical optics, and quantum photonics.

Here, we present experimental insertion loss (IL) and group delay (GD) measurements of compact and cascadeable silicon microring filters, as shown in Fig. 1, which achieve record 100 dB contrast (two cascaded 5-ring sections) in the drop port for a single (transverse-electric, TE) polarization, as conventionally used in microrings based on rectangular cross-section nanophotonic silicon wire waveguides. Furthermore, we demonstrate electrical current driven thermo-optic tuning of the passband width (one edge fixed) from 125 GHz to 11.6 GHz.

Manuscript received April 22, 2013; revised May 14, 2013 and May 29, 2013; accepted June 4, 2013. Date of publication June 10, 2013; date of current version July 22, 2013. This work was supported by the National Science Foundation under Grants ECCS 092539, 1028553, 1153716, 1201308, and the CIAN ERC EEC-0812072. The work of J. R. Ong was supported by the Agency for Science, Technology and Research, Singapore.

The authors are with the Department of Electrical and Computer Engineering, University of California, San Diego, CA 92093 USA (e-mail: j5ong@ucsd.edu; rkumar@ucsd.edu; mookherjea@ece.ucsd.edu).

Color versions of one or more of the figures in this letter are available online at http://ieeexplore.ieee.org.

Digital Object Identifier 10.1109/LPT.2013.2267539

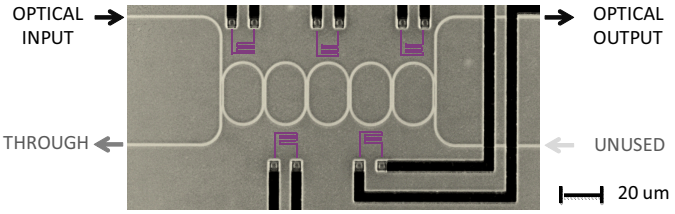

Fig. 1. Optical microscope image of a nearest-neighbor coupled 5-ring silicon filter, using rings in the racetrack configuration and directional waveguide couplers between adjacent rings, with the input and output single-mode silicon nanophotonic waveguides indicated. On-chip resistive micro-heaters, defined by doped silicon wires and not visible in a microscope image, are indicated with dark blue lines. One filter stage achieved 50 dB contrast and two such filter stages were cascaded to form a tunable-bandwidth multi-channel filter and achieved 100 dB contrast.

II. Experimental Procedure

The devices were fabricated using complementary metal-oxide-semiconductor compatible processes on silicon-on-insulator wafers at the Institute of Microelectronics (Singapore), and singulated into chips for testing using edge-coupled waveguide-to-fiber tapers. The insertion loss of each fiber-to-waveguide coupler was estimated as 4.3 dB averaged over the wavelengths of interest, based on calibration measurements on separate test sites. The single-mode waveguides, with width 0.55 μm, height 0.22 μm, and slab thickness 70 nm, were designed for low loss (approx. 2 dB/cm) transverse electric (TE) polarization transmission relative to the device plane. The microring resonators were in the racetrack configuration, with radius 10 μm and directional coupler length 10 μm. Within each section of 5 rings, the rings were nominally identical, with apodized waveguide-resonator coupling coefficients, formed by varying the inter-waveguide gap in the directional couplers, from 210 nm for the first and last couplers to 320 nm in the middle. Microheaters were formed using doped, zig-zag shaped line in the silicon slab, with width 0.5 μm and height 70 nm, situated about 2 μm from the silicon waveguide forming the ring. On one representative chip, the average heater resistance was 20 kΩ, with a standard deviation of 4.3 kΩ.

The intensity transmission and group delay were measured using an optical vector network analyzer (OVA) instrument, manufactured by Luna Technologies (Blacksburg, VA). The measurement technique is that of swept-wavelength interferometry, a homodyne measurement method which achieves high sensitivity and amplified spontaneous emission

noise rejection. The procedures used to calculate transmission and group delay from the measured Jones matrix, and calibration against a known standard (e.g., acetylene gas cell), are described in Ref. [14].

In the measurement setup, the total laser-to-detector insertion loss was about 19 dB, including four waveguide-to-fiber couplers with insertion loss 4.3 dB each. To overcome the coupling losses and maintain a high signal-to-noise ratio at the detector, the output of the OVA (average power 200 μW) was amplified (before the chip) by an erbium-doped fiber amplifier (EDFA), which was used in the saturation regime, followed by a programmable passive attenuator to reduce the power level incident on the silicon chip to a sufficiently low level to avoid nonlinearities. No amplification was performed after the chip. Calibration measurements showed that the EDFA and attenuator combination added negligible noise to the measurements when averaging over multiple data sets is performed, since such averaging results in the residual IL and GD ripple converging to the true device ripple as the number of acquired traces increases [15].

Transmission was calculated from the eigenvalues of the matrix $\mathbf{J}^{\dagger}(\omega)\mathbf{J}(\omega)$, where $\mathbf{J}(\omega)$ is the measured Jones matrix of the filter at radian frequency ω. At a given frequency, the greater eigenvalue represents the maximum transmission polarization state, and the smaller eigenvalue represents the minimum transmission polarization state [16]. By comparing with a transfer-matrix calculation of the coupled-ring transmission spectrum, we were able to identify which measured polarization corresponded to the TE polarization. The weakly-transmitted transverse magnetic (TM) polarized light is spectrally flat, with some incidental ripples not related to the free spectral range (FSR) of the microring; this behavior has also been seen in single-ring filters [17, Fig. 7(b)].

III. Measurements

A. Single Stage (5 Ring, Fixed Bandwidth)

Fig. 2 shows a wide-wavelength-range transmission measurement through a single 5-ring silicon filter stage. Transmission of both TE and TM polarizations is shown; the former is the quantity of interest as the rings and couplers were designed using the group index of the TE polarization in mind, and silicon nanophotonic waveguides are significantly birefringent [18]. For a representative channel near 1550 nm, the measured insertion loss of the 5-ring filter was 1.4 dB, and group delay ripple (GDR) was less than 3 ps over 125 GHz bandwidth. From one band to the next, transmission uniformity of each passband was seen over a wide range of wavelengths, extending throughout the C and L telecommunications bands (1530–1610 nm), since the standard deviation of the average band-center insertion loss across 11 passbands was only 0.96 dB. The FSR of the microrings was 7.3 nm near 1550 nm. The systematic increase in the edge-to-edge passband width versus wavelength, from 1.69 nm at 1531 nm to 2.39 nm near 1606 nm, was due to the dispersion of typical silicon waveguide directional couplers [19], with $|\kappa|$ varying monotonically from 0.366 to 0.464 over those wavelengths.

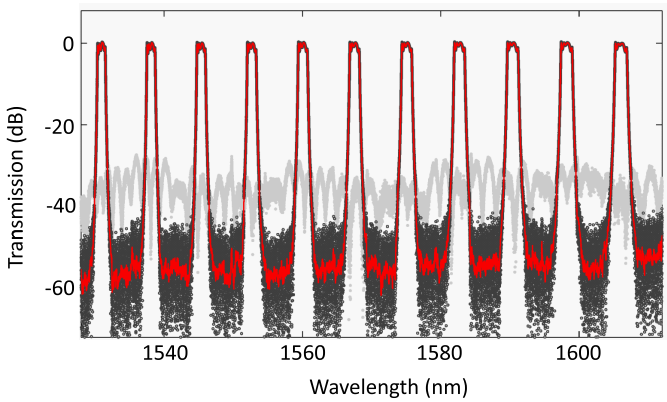

Fig. 2. Transmission of a single filter stage (5 rings) measured from 1530 to 1610 nm. The TE polarization, which is the quantity of interest, in view of the waveguide and coupler design, is shown in dark gray colored dots (raw measurement) and after moving-window smoothing filter of span 50 pm (shown using a red line). Transmission in the TM polarization is shown using a light gray colored line.

B. Dual Stage (10 Ring, Coincident Passbands)

A 10-ring filter cascade was obtained by cascading two 5-ring structures, each on a separate chip. When the center wavelength of one group of five rings was thermally shifted relative to the other, the bandwidth could be narrowed without greatly degrading the ripple characteristics. We ensured that TE polarization was used at the input of both chips. The additional interconnection incurred an additional 9 dB insertion loss, but did not impact the measurement of either contrast or bandwidth.

The TE-polarized transmission through the dual-stage filter is shown in Fig. 3(a). High-dynamic range measurement of one passband is shown in Fig. 3(b). At the lowest transmission level, data taken with 1.2 pm wavelength resolution (hardware limit) is shown with grey dots, and was subject to instrumental noise, as verified with a measurement of a fiber patch-cable replacing the silicon chip. The yellow line was obtained by a moving-window smoothing filter of span 50 pm; since averaging repeated measurements, or increasing the smoothing filter window, did not reduce the noise floor, this yellow line was attributed to the device under test and defined the transmission floor. 100 dB contrast was measured with regard to this floor; 90 dB contrast was obtained with regard to the unfiltered instrumental-noise-defined floor. As shown in Fig. 3(c), less than 3 dB insertion loss ripple was obtained over a bandwidth of 100 GHz. As shown in Fig. 3(d), the GDR was less than 5 ps over a continuous 75 GHz bandwidth near the band-center. GDR was well fit by a simple polynomial chromatic dispersion profile.

C. Dual Stage (10 Ring, Separated Passbands)

The thermo-optic (red) shift of the refractive index can be used to spectrally shift the resonance wavelengths, as shown in Fig. 4(a). Using current driven through the on-chip microheater, with tuning efficiency 1.25 GHz/mW, a tuning range of approx. 50 GHz was seen before heater damage. Device failure occurred relatively easily in the present design

TABLE I
RECENT RESULTS OF MULTI-ELEMENT CHIP-SCALE SILICON FILTERS (CHANNEL DROP)

	Filter order	BW_{max} / FSR	Tunable BW	Insertion loss (dB/element)	Contrast
Popovic et al. (2007) [10]	4	66 GHz / 2 THz	No	0.37 dB	32 dB
Xia et al. (2007) [5]	5	310 GHz / 18 nm	No	0.36 dB	40 dB
Dong et al. (2010) [7]	5	1.9 GHz / 50 GHz	No	0.7 dB	50 dB
Ibrahim et al. (2011) [8]	4	0.4 GHz / 10 GHz	0.6–2 GHz	0.6 dB	30 dB
Alipour et al. (2011) [11]	4	5 GHz / 650 GHz	0.9–5 GHz	1.25–3.75 dB	38 dB
Ding et al. (2011) [12]	2 rings + MZI	55 GHz / 1 THz	28–55 GHz	3.6 dB (total)	30 dB
Orlandi et al. (2012) [13]	2 rings + MZI	173 GHz / 200 GHz	23–173 GHz	0.46 —1.06 dB (total)	15–34 dB
Luo et al. (2012) [6]	10	100 GHz / 750 GHz	No	0.3 - 0.6 dB	50 dB
Ong et al. (2013) (this work)	5 and 10	125 GHz / 0.9 THz	11.6–125 GHz	0.28 dB	50 dB and 100 dB

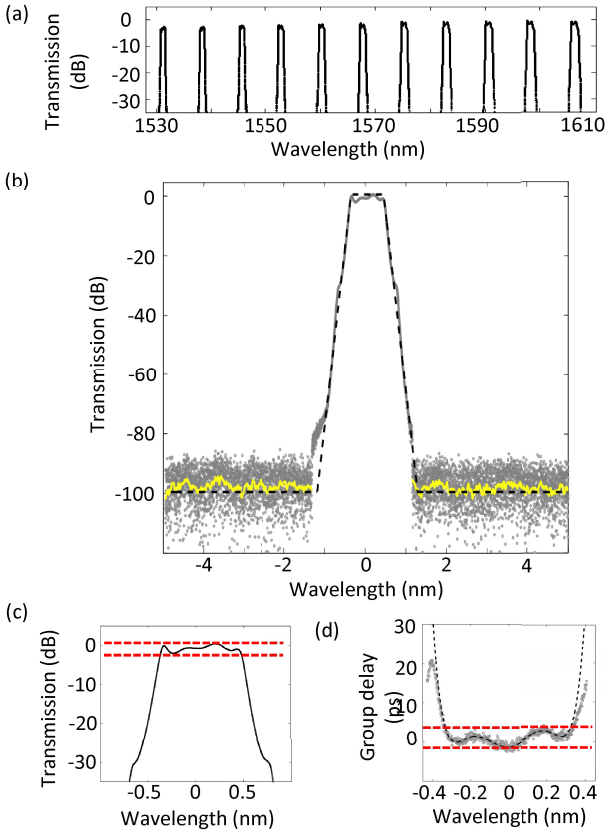

Fig. 3. (a) Transmission of a dual-stage (10 microring) filter in the TE polarization. (b) High dynamic range measurement of a passband near 1.55 μm, using amplified swept-wavelength interferometry, with the yellow line representing the averaged (50 pm) noise floor of the raw instrumental data shown with gray dots, and the dashed line as a visual guide to the filter roll-off, with slope 119 dB/nm. (c) Dashed lines show the margins of 3 dB IL ripple extending over 125 GHz spectral bandwidth. (d) Dashed lines show 5 ps bounds for the measured GD ripple near the band-center over 75 GHz bandwidth, indicating a level of GDR in the as-fabricated device, without trimming, comparable to cascaded fiber Bragg grating devices. GDR was fit by a simple polynomial chromatic dispersion profile.

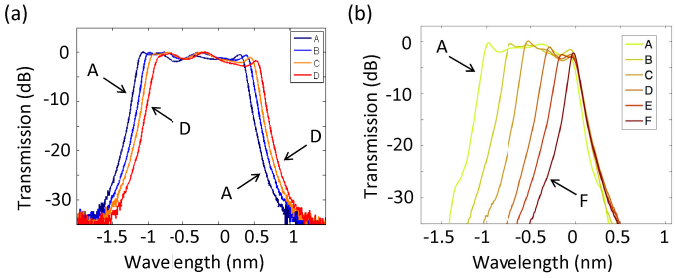

Fig. 4. (a) Using on-chip microheaters, the passband of one 5-ring filter section was red-shifted, as shown in this low-dynamic-range measurement. Heater drive powers for A, B, C and D are 0 mW, 9.3 mW, 15 mW and 22 mW. (b) For a cascaded filter, the 3-dB bandwidth was reduced from Δf_{FWHM} = 125 GHz to 11.6 GHz, by tuning the temperature of one section of five rings relative to the other (held constant at 23.2 °C), with relative temperature increase, ΔT at A = 0 °C, B = 3 °C, C = 5.6 °C, D = 8.5 °C, E = 10.2 °C and F = 12 °C. To achieve a larger range of temperature shifts than in Fig. 4(a), the chip temperature was controlled using a thermo-electric module and temperatures were estimated using a measurement of resistance and a thermistor equation.

because the heaters were implemented using doped silicon meanders in the thin silicon slab, and were intended for fine-tuning the ring resonances, not large-range band shifting. However, a greater range of tuning (>100 GHz) was possible by heating the chip itself through a thermo-electric module. In a cascaded configuration, when one set of rings was thermally shifted relative to the other, the composite filter bandwidth of each channel was reduced. The longer-wavelength edge of the cascaded passband stays fixed, and the shorter-wavelength edge of the passband is moved closer towards the other edge; such functionality is needed for filtering of a variable number of discrete channels in a telecommunication network, among other applications. Full pole-zero tunability, as shown by other work [8], is not needed for such filtering; here, a single control voltage is sufficient to tune the bandwidth. Shown in Fig. 4(b) are snapshots of a representative transmission passband reduced from 125 GHz to 11.6 GHz, i.e., more than a 10× range, at discrete points along the tuning curve.

IV. DISCUSSION

Table I summarizes some of the best-performing silicon photonic multi-stage filters made using a variety of different approaches; some combine multiple elements (rings and Mach-Zehnder interferometer) in a single stage, some offer full control over poles and zeros whereas others (like ours) demonstrate tunable bandwidth via simpler means. Some designs offer electro-optic tunability, whereas others demonstrate thermo-optic tunablity. Taken together, these results show silicon photonic chip-scale multi-stage filters evolving to show a level of performance approaching that of much larger, table-top instruments in most metrics.

Now, we discuss some fundamental aspects for further improving contrast in a multi-ring cascade. Light propagates along the axial coordinate of the device z with exponential attenutation, i.e., $\exp(-\alpha z)$ for passband and stopband wavelengths, but with small and large values of α in the two cases. For passband wavelengths, the loss coefficient [20] $\alpha = \alpha_{\mathrm{wg}} \pi R/|\kappa|$ in terms of the propagation loss of a silicon nanophotonic waveguide, which constitutes the racetrack resonators, and has a loss coefficient $\alpha_{\mathrm{wg}} \approx 2$ dB.cm^{-1}, the bending radius R, and the magnitude of the inter-ring coupling coefficient $|\kappa|$. For stop-band wavelengths, the propagation coefficient can be estimated by Bloch's theory with a complex propagation coefficient, and is $\alpha = -\cosh^{-1}(1/|\kappa|)$. Therefore, for an N-ring chain, ignoring apodization, the contrast is

$$\frac{T_{\mathrm{passband}}}{T_{\mathrm{stopband}}} = \frac{\exp\left[-\alpha_{\mathrm{wg}} \pi R N/|\kappa|\right]}{\exp\left[-N \cosh^{-1}(1/|\kappa|)\right]}. \quad (1)$$

The subtlety in Eq. (1) is that recent simulation and experimental studies [21] on realistic (i.e., with disorder effects) silicon coupled microrings suggest that the number of resonators N that can be coupled in a disorder-free manner is not independent of $|\kappa|$, but is proportional to $|\kappa|^2$. Then, a robust strategy to achieve high contrast is to *increase* the coupling coefficient: A larger $|\kappa|$ reduces the contrast in a single-stage filter, but the overall contrast can be increased by supporting longer chains of resonators than possible in the small-$|\kappa|$ case. Another advantage of a higher value of $|\kappa|$ is that the filter has a greater transmission bandwidth, and therefore, a wider tunable bandwidth range in the case of the cascaded-filter scheme shown here.

V. Conclusion

In conclusion, our results demonstrate measurement of record contrast between in-band and stop-band transmission, along with good band-to-band uniformity, simple thermo-optic bandwidth tunability, low group delay ripple and low (on-chip) insertion loss, using compact coupled microrings in silicon photonics. High-performance, high-contrast tunable bandwidth filtering is available only in much larger, bench-top systems today (Finisar WaveShaper, Santec OTF etc.) and chip-scale filter technology can benefit flexible bandwidth channel plans in next-generation optical networks, improved noise rejection in tunable lasers and receivers, isolating wavelength conversion products and blocking residual pump light, improving the quantum visibility of photon pairs generated by spontaneous nonlinear optical processes, etc.

Acknowledgment

The authors are grateful to X. Luo, T.-Y. Liow, and G.-Q. P. Lo (IME, Singapore) for discussions and help with device fabrication, and D. K. Gifford (Luna Technologies) for assistance with the OVA.

References

[1] S. T. Chu, B. Little, W. Pan, T. Kaneko, and Y. Kokubun, "Cascaded microring resonators for crosstalk reduction and spectrum cleanup in add-drop filters," *IEEE Photon. Technol. Lett.*, vol. 11, no. 11, pp. 1423–1425, Nov. 1999.

[2] H. Shen, *et al.*, "Eight-channel reconfigurable microring filters with tunable frequency, extinction ratio and bandwidth," *Opt. Express*, vol. 18, no. 17, pp. 18067–18076, 2010.

[3] M. S. Dahlem, C. W. Holzwarth, A. Khilo, F. X. Kärtner, H. I. Smith, and E. P. Ippen, "Reconfigurable multi-channel second-order silicon microring-resonator filterbanks for on-chip WDM systems," *Opt. Express*, vol. 19, no. 1, pp. 306–316, 2011.

[4] E. J. Klein, *et al.*, "Densely integrated microring resonator based photonic devices for use in access networks," *Opt. Express*, vol. 15, no. 16, pp. 10346–10355, 2007.

[5] F. Xia, M. Rooks, L. Sekaric, and Y. Vlasov, "Ultra-compact high order ring resonator filters using submicron silicon photonic wires for on-chip optical interconnects," *Opt. Express*, vol. 15, no. 19, pp. 11934–11941, 2007.

[6] X. Luo, *et al.*, "Silicon high-order coupled-microring-based electro-optical switches for on-chip optical interconnects," *IEEE Photon. Technol. Lett.*, vol. 24, no. 10, pp. 821–823, May 15, 2012.

[7] P. Dong, *et al.*, "GHz-bandwidth optical filters based on high-order silicon ring resonators," *Opt. Express*, vol. 18, no. 23, pp. 23784–23789, 2010.

[8] S. Ibrahim, *et al.*, "Demonstration of a fast-reconfigurable silicon CMOS optical lattice filter," *Opt. Express*, vol. 19, no. 14, pp. 13245–13256, 2011.

[9] M. Attygalle, N. Nadarajah, and A. Nirmalathas, "Wavelength reused upstream transmission scheme for WDM passive optical networks," *Electron. Lett.*, vol. 41, no. 18, pp. 1025–1027, 2005.

[10] M. A. Popovic, *et al.*, "Tunable, fourth-order silicon microring-resonator add-drop filters," in *Proc. 33rd Eur. Conf. Exhibit. Opt. Commun.*, 2007, pp. 1–2.

[11] P. Alipour, *et al.*, "Fully reconfigurable compact RF photonic filters using high-Q silicon microdisk resonators," *Opt. Express*, vol. 19, no. 17, pp. 15899–15907, 2011.

[12] Y. Ding, *et al.*, "Bandwidth and wavelength-tunable optical bandpass filter based on silicon microring-MZI structure," *Opt. Express*, vol. 19, no. 7, pp. 6462–6470, 2011.

[13] P. Orlandi, *et al.*, "Reconfigurable silicon filter with continuous bandwidth tunability," *Opt. Lett.*, vol. 37, no. 17, pp. 3669–3671, 2012.

[14] D. K. Gifford, B. J. Soller, M. S. Wolfe, and M. E. Froggatt, "Optical vector network analyzer for single-scan measurements of loss, group delay, and polarization mode dispersion," *Appl. Opt.*, vol. 44, no. 34, pp. 7282–7286, 2005.

[15] M. Cooper, M. Schneider, G. Gupta, and S. Mookherjea, "Filter-less amplification for rapid swept-wavelength interferometric measurement of silicon waveguide group delay statistics," *IEEE Photon. Technol. Lett.*, vol. 23, no. 12, pp. 783–785, Jun. 15, 2011.

[16] B. Heffner, "Automated measurement of polarization mode dispersion using jones matrix eigenanalysis," *IEEE Photon. Technol. Lett.*, vol. 4, no. 9, pp. 1066–1069, Sep. 1992.

[17] H. Fukuda, K. Yamada, T. Tsuchizawa, T. Watanabe, H. Shinojima, and S. Ichi Itabashi, "Silicon photonic circuit with polarization diversity," *Opt. Express*, vol. 16, no. 7, pp. 4872–4880, 2008.

[18] E. Dulkeith, F. Xia, L. Schares, W. M. J. Green, and Y. A. Vlasov, "Group index and group velocity dispersion in silicon-on-insulator photonic wires," *Opt. Express*, vol. 14, no. 9, pp. 3853–3863, 2006.

[19] R. Aguinaldo, Y. Shen, and S. Mookherjea, "Large dispersion of silicon directional couplers obtained via wideband microring parametric characterization," *IEEE Photon. Technol. Lett.*, vol. 24, no. 14, pp. 1242–1244, Jul. 15, 2012.

[20] J. K. S. Poon, J. Scheuer, Y. Xu, and A. Yariv, "Designing coupled-resonator optical waveguide delay lines," *J. Opt. Soc. Amer. B*, vol. 21, no. 9, pp. 1665–1673, 2004.

[21] S. Mookherjea and M. A. Schneider, "Avoiding bandwidth collapse in long chains of coupled optical microresonators," *Opt. Lett.*, vol. 36, no. 23, pp. 4557–4559, 2011.